THE GERONTOLOGICAL SOCIETY OF AMERICA®

Journals of Gerontology: Biological Sciences
cite as: *J Gerontol A Biol Sci Med Sci*, 2017, Vol. 72, No. 6, 763–770
doi:10.1093/gerona/glw170
Advance Access publication August 29, 2016

OXFORD

Original Article

DNA Damage Detection by 53BP1: Relationship to Species Longevity

Eleonora Croco,[1] Silvia Marchionni,[2] Martine Bocchini,[2] Cristina Angeloni,[1] Thomas Stamato,[3] Claudio Stefanelli,[1] Silvana Hrelia,[1] Christian Sell,[4] and Antonello Lorenzini[2]

[1]Department for Life Quality Studies and [2]Department of Biomedical and Neuromotor Sciences, University of Bologna, Italy. [3]The Lankenau Institute for Medical Research, Wynnewood, Pennsylvania. [4]Department of Pathology, Drexel University College of Medicine, Philadelphia, Pennsylvania.

Address correspondence to Antonello Lorenzini, PhD, Department of Biomedical and Neuromotor Sciences, University of Bologna, Via Irnerio 48, 40126 Bologna, Italy. E-mail: antonello.lorenzini@unibo.it

Received March 11, 2016; Accepted August 8, 2016

Decision Editor: Rafael de Cabo, PhD

Abstract

In order to examine potential differences in genomic stability, we have challenged fibroblasts derived from five different mammalian species of variable longevity with the genotoxic agents, etoposide and neocarzinostatin. We report that cells from longer-lived species exhibit more tumor protein p53 binding protein 1 (53BP1) foci for a given degree of DNA damage relative to shorter-lived species. The presence of a greater number of 53BP1 foci was associated with decreased DNA fragmentation and a lower percentage of cells exhibiting micronuclei. These data suggest that cells from longer-lived species have an enhanced DNA damage response. We propose that the number of 53BP1 foci that form in response to damage reflects the intrinsic capacity of cells to detect and respond to DNA harms.

Keywords: 53BP1—DNA damage foci—Genomic stability—Longevity—Micronuclei

Introduction

Double-strand breaks (DSBs) are the most harmful DNA lesions a cell can encounter. In mammals, nonhomologous end-joining is the cellular mechanism responsible for repairing the majority of DSBs (1). This is because nonhomologous end-joining is much faster than homologous recombination (2), and it is active throughout the cell cycle, whereas homologous recombination is typically active only during the S and G_2 phases (3). Moreover, the majority of cells in the adult body are in G_0. At the sites of DSBs, nuclear foci of phosphorylated histone H2AX (γ-H2AX) and tumor protein p53 binding protein 1 (53BP1) can be detected by immunofluorescence and are widely used as DNA damage markers because their abundance has been reported to correlate very closely with the degree of genotoxic insult (reviewed in ref. (4)). 53BP1 accumulates in DNA damage foci after the occurrence of DSBs in order to facilitate nonhomologous end-joining repair (5). Previous works had shown that 53BP1 is involved in activation of the DNA damage response during the G_1, S, and G_2 phases of the cell cycle (6–8).

We have previously observed an unexpected difference in the formation of DNA damage foci between human and mouse cells following exposure to the same concentration of neocarzinostatin (NCS). Despite similar exposure to the DNA-damaging agent, human cells exhibited a significantly greater number of 53BP1 foci compared with mouse cells. The greater abundance of foci in human cells correlated inversely with the appearance of micronuclei, which represent the presence of severe genomic damage (9). We have also reported an impressive correlation between mammalian longevity and the capacity of nuclear proteins to bind DNA ends, which appears to be largely dependent on increased expression of the evolutionarily highly conserved heterodimer Ku80/Ku70 (10). The DNA end-binding assay represents the accumulation of proteins required for the initial DNA damage recognition, a necessary step before a cell can proceed with repair, cell cycle arrest, or apoptosis. These data persuaded us to conduct a deeper investigation into the relationship between the appearance of markers of DNA damage and mammalian longevity.

To this end, we have compared fibroblast cells from mouse (maximum life span, 4 years; weight, 20.5 g), cow (maximum life span, 20 years; weight, 750 kg), dog (maximum life span, 24 years; weight, 40.0 kg), little brown bat (maximum life span, 34 years; weight, 10.0 g), and human (maximum life span, 122 years; weight, 62.0 kg) in their response to the genotoxic insult caused by etoposide (ETO) and NCS. ETO is a poison that binds reversibly to topoisomerase IIα/β to block religation of cleaved DNA strands, causing DSBs (11), whereas NCS is a macromolecular chromoprotein antibiotic that causes single-strand breaks and DSBs (12). Our experimental approach was based on the assumption that the biological mechanisms that facilitate longevity are cell autonomous and thus will be reflected in fundamental cellular processes. Consequently, these mechanisms can be studied in cell culture away from the complexity of the whole organism. For example, using a cell culture approach, Dostál and colleagues have demonstrated that long-lived rodent species are more efficient in excluding cadmium that is known for disturbing DNA base excision and mismatch repair (13).

With the present work, we propose that quantitative species-specific differences in 53BP1 foci formation, observed following exposure to genotoxic agents, correlate with differences in life span and adult body mass, suggesting a new interpretation of nuclear foci as markers of a species' ability to detect and mitigate DNA damage to ensure genomic stability.

Material and Methods

Cell Culture

All fibroblast strains and lines used are described in Supplementary Table 1. Fibroblast strains from mouse, little brown bat, dog, and cow were established as previously described (14). Adult human fibroblasts were obtained from Claudio Franceschi (DIMES, University of Bologna, Italy).

Cells were maintained in minimum essential medium with Earle's salts and l-glutamine containing 10% fetal bovine serum, minimum essential medium vitamins and amino acids, and penicillin–streptomycin (all from Sigma–Aldrich, St Louis, MO). Fibroblasts were passaged weekly, and cumulative population doubling was determined as previously described (15). With the exception of the immortalized 3T3 mouse line and little brown bat strains that had undergone spontaneous immortalization, lines displayed replicative senescence and were used for all experiments at approximately half way through their replicative life span.

Genotoxic Treatment

Cells were treated with ETO and NCS (both from Sigma–Aldrich). The majority of the experiments were performed on S-phase synchronized cells, and when unsynchronized cells were used, this is specified in the text. S phase was chosen as the most appropriate time for exposure to genotoxic stress because a previous study determined that differences in susceptibly to genotoxic damage between human and mouse cells were most apparent in S–G_2 (9). In addition, topoisomerase II inhibitors are most effective during DNA replication (16). Cultures were initially arrested in G_0 by serum starvation for 48 hours in serum-free medium. Cells were then stimulated to enter the cell cycle by the addition of fresh complete medium with 10% fetal bovine serum (FBS). For each species, the time following fetal bovine serum stimulation required for entry into S phase was defined by cell cycle analysis (data not shown). Mouse and bat cells were stimulated in complete medium with 10% fetal bovine serum for 16 hours, and dog, cow, and human for 18 hours. Once synchronized, cells were treated in complete serum-free medium to avoid the potential for interference of serum on drug bioavailability. Unsynchronized cells were used only on initial dose–response experiments (Supplementary Figures 1 and 2). Doses ranging from 5 to 100 μM of ETO and 0.13 to 1.35 μM of NCS were used.

Immunofluorescence Determination of 53BP1, γ-H2AX, and Promyelocytic Leukemia Protein Foci

Fibroblasts were seeded onto glass coverslips and treated with ETO or NCS at varying concentrations for 6 or 2 hours, respectively. Cells were fixed at the indicated times after the beginning of damage in 4% paraformaldehyde for 10 minutes and permeabilized in 0.2% Triton X-100 in phosphate-buffered saline (PBS) for 5 minutes. Cells were washed once in PBS and blocked for 30 minutes in 4% bovine serum albumin (BSA) in PBS containing Tween-20 (PBST), after which they were incubated with primary antibody (53BP1, NB 100–304 or NB 100–305, Novus Biologicals, Littleton, CO; γH2AX, 05-636, clone JBW301, Merck Millipore, Billerica, MA; PML Antibody [PG-M3]: sc-966, Santa Cruz, Dallas, TX) in 1% BSA–PBST buffer for 1 hour at room temperature in a humidified chamber. Anti-53BP1 antibody (NB 100–304) binds, in tested species, epitopes with homologies that range between 90% and 92% compared to the human epitope. Anti-γ-H2AX antibody, used for human and mouse, binds an epitope with a homology of 90% between these two species. Slides were washed three times in PBST and incubated with AlexaFlour555-conjugated goat anti-rabbit and AlexaFluor488-conjugated goat anti-mouse secondary antibody (respectively, #4413S and #4408S; Cell Signaling, Danvers, MA) in 1% BSA–PBST for 1 hour. Cells were washed three times, stained with 4′,6-diamidine-2′-phenylindole dihydrochloride (DAPI, Sigma–Aldrich), and mounted with Vectashield mounting medium (Vector Laboratories, Burlingame, CA) before analysis. Images were captured using an Olympus BX61 fluorescence microscope (Tokyo, Japan) equipped with a Hamamatsu ORCA-ER camera (Hamamatsu City, Japan) or an Olympus IX50 equipped with a Diagnostic Instruments 9.0 Monochrome-6 camera (Sterling Heights, MI). Clearly identifiable 53BP1 or γ-H2AX foci inside the nucleus were counted as positive foci. Nuclei were scored as containing: 53BP1 foci (F) < 5; 5 ≤ F < 20; F ≥ 20. Nuclei with fewer than five foci were considered foci negative because this number of foci was common in untreated cells. Overlapping and/or contiguous 53BP1 and promyelocytic leukemia protein (PML) foci were scored in colocalization experiments.

Micronuclei Assay

Cells synchronized in S phase as previously described were treated with ETO or NCS at varying concentrations for 6 or 2 hours, respectively. At the times indicated in each figures, cells were fixed in 4% paraformaldehyde for 10 minutes and permeabilized in 0.2% Triton X-100 in PBS for 1 minute. Fixed cells were stained with DAPI and washed with PBS. Cells were mounted with Vectashield and scored using fluorescence microscopy as above. Micronuclei, defined as DAPI-positive bodies that were morphologically identical but smaller than the nucleus, were scored according to Thomas and Fenech (17). Cells were considered micronucleus positive if they contained, at least, one micronucleus.

DNA Synthesis Assessment

Fibroblasts were seeded onto glass coverslips, synchronized as described above, and treated with 5 μM ETO for 6 hours. About 10 μM 5-bromo-2′-deoxyuridine (BrdU) pulse, with different

lapse of time, was performed to assess DNA synthesis. Cells were fixed at the desired time point, as previously described, and were treated with 1 M HCl for 45 minutes at room temperature. HCl was then neutralized with borate buffer, and cells were washed once in PBS and blocked for 30 minutes in 4% BSA in PBST. Cells were incubated with an anti-BrdU antibody (clone BU20A; eBioscience, San Diego, CA) in 1% BSA–PBST buffer for 2 hours at 37°C in a humidified chamber. Slides were then washed three times in PBST and incubated in AlexaFluor488-conjugated goat anti-mouse secondary antibody in 1% BSA–PBST for 1 hour to label BrdU incorporation.

Comet Assay

The microgel electrophoretic technique was performed utilizing the neutral lysis method that detects DSBs (18). From a population of synchronized cells, a single-cell suspension was prepared by trypsin disaggregation. Disaggregated cells were counted and treated with 50 µM ETO and 1.35 µM NCS, respectively, for 60 and 30 minutes, at room temperature and were then resuspended in 1% low-melting agarose. The low-melting cellular suspension was seeded onto slides, and cells were lysed by placing the slides in a humid chamber at 37°C with 2% sodium dodecyl sulfate (SDS), 0.05 M ethylenediaminetetraacetic acid (EDTA), and 0.5 mg/mL proteinase K for at least 18 hours. Lysis was performed under neutral conditions to detect DSBs. After lysis, slides were washed two times in 0.5× Tris/Borate/EDTA (TBE) buffer. Electrophoresis was carried out at 30 V/cm for 15 minutes in 0.5× TBE buffer. For visualization of DNA damage, slides were stained with DAPI and observed using fluorescence microscopy as described above. Cells with DNA damage appeared as comets. One hundred comets were scored for each species and each time point, and analyzed with Open Comet (19) image analysis software. Individual comet images were scored for several features including tail length and percentage DNA in tail.

Cellular Viability Assay

Fibroblast viability was evaluated in terms of mitochondrial activity, by conversion of the dye 3-(4,5-dimethylthiazol-2-yl)-2,5-diphenyltetrazolium bromide (MTT) to insoluble formazan (20). Cells were seeded in 96-well plates and treated with 5 and 50 µM of ETO and 0.13 and 1.35 µM of NCS for 6 and 2 hours, respectively. At the times indicated (24, 48, and 72 hours), cells were washed with PBS and incubated in MTT (5 mg/mL) in PBS for 2 hours. After removal of MTT, formazan crystals were dissolved with dimethyl sulfoxide (DMSO; all from Sigma–Aldrich) and the amount of formazan was measured at λ = 570 nm (ref. λ = 690 nm) with a spectrophotometer (Victor^2 Multilabel Counter, PerkinElmer, Waltham, MA). All experiments were repeated at least two times, with each comprising an evaluation of five wells per treatment. Mitochondrial activity in treated cells was calculated as a percentage relative to control cells according to the formula: (absorbance of treated fibroblasts/absorbance of untreated fibroblasts) × 100.

Statistical Analysis

All statistical analyses were performed using Graphpad Software (La Jolla, CA). Maximum human longevity is 122 years. In the figure captions and in the correlation analysis, it is adjusted to 90 years to account for the fact that, for the others species, only small cohorts were used to determine maximum life span, and 90 years seem a more realistic estimate for a random sample of humans.

Results

Dose–Response Experiments in 53BP1 Foci Formation

In preliminary experiments, increasing doses of genotoxics were used to determine time and concentrations that would yield a not-maximized 53BP1 foci response. Supplementary Figure 1 reports data from one experiment on human cells exposed to increasing concentration of NCS for 2 hours. Already at a concentration of 0.22 µM NCS, the 53BP1 foci response is maximized (ie, the vast majority of nuclei have more than 20 53BP1 foci each; Supplementary Figure 1C). At the highest concentration used of NCS (1.35 µM), while the response of the most responsive species (human) was totally maximized, the response of mouse cells were still intermediate (see Supplementary Figure 2). Similar dose–response experiments were performed for ETO (see Supplementary Figure 8A) that is a less potent genotoxic than NCS (see comet assay result in Figure 3). The majority of the experiments, in the present work, were carried out using the lowest concentration capable of elicit a significant response.

53BP1 Foci Formation Across Species

For the majority of the experiments presented here, cells were exposed to either 5 µM ETO or 0.13 µM NCS during S phase and were monitored at specific time intervals, up to 3 days after the beginning of damage. Figure 1A presents data from cells treated with 5 µM ETO. Time-course analysis after 5 µM ETO treatment revealed a peak in 53BP1 foci formation between 2 and 10 hours in all species (Figure 1C), followed by a gradual decline in the percentage of foci-positive nuclei. Interestingly, longer-lived species showed a higher percentage of nuclei with 53BP1 foci. Human cells, derived from the longest-lived species, exhibited the highest percentage of foci when compared to all other species, with statistical significance observed consistently at 2 and 24 hours from the beginning of damage. Moreover, human cells seemed to retain a higher number of foci over time. Because we previously observed that 24 hours was required for visible foci to form in cells treated with 1.5 µg/mL of NCS (0.13 µM) (9), we scored foci from 24 to 72 hours after the beginning of damage with this agent. Similar to results with 5 µM ETO treatment, longer-lived species exhibited a higher percentage of cells with more than five foci per nucleus in response to 0.13 µM NCS. Human cells showed the highest percentage of cells with more than five 53BP1 foci (Figure 1B and D). At the opposite, both primary and immortalized 3T3 mouse cells exhibited the lowest foci response among the studied species; mouse and cow response were comparable only in the case of ETO treatment. To monitor cell survival under these conditions, we also measured metabolic activity as the capacity to convert MTT to formazan (Figure 2). Low-dose treatments (5 µM ETO or 0.13 µM NCS) did not cause a significant reduction in MTT activity, whereas doses 10 times higher did.

Colocalization of 53BP1 With γ-H2AX

Because our previous data suggest that long-lived species have a better Ku70-Ku80 DNA-end biding capacity (10), we speculated that long-lived species could be more efficient in detecting and possibly repairing DNA DSBs. To prove that our treatments were able to elicit DSBs, we performed coimmunostaining experiments for 53BP1 and γ-H2AX. This colocalization is, in fact, an accepted marker of the presence of a DSB (21). Supplementary Figure 3A shows that, with 5 µM ETO treatment, 53BP1 foci colocalize with γ-H2AX foci in the vast majority of cases, in both mouse primary and human cells. Between 1, 2, and 10 hours after the beginning of treatment, every

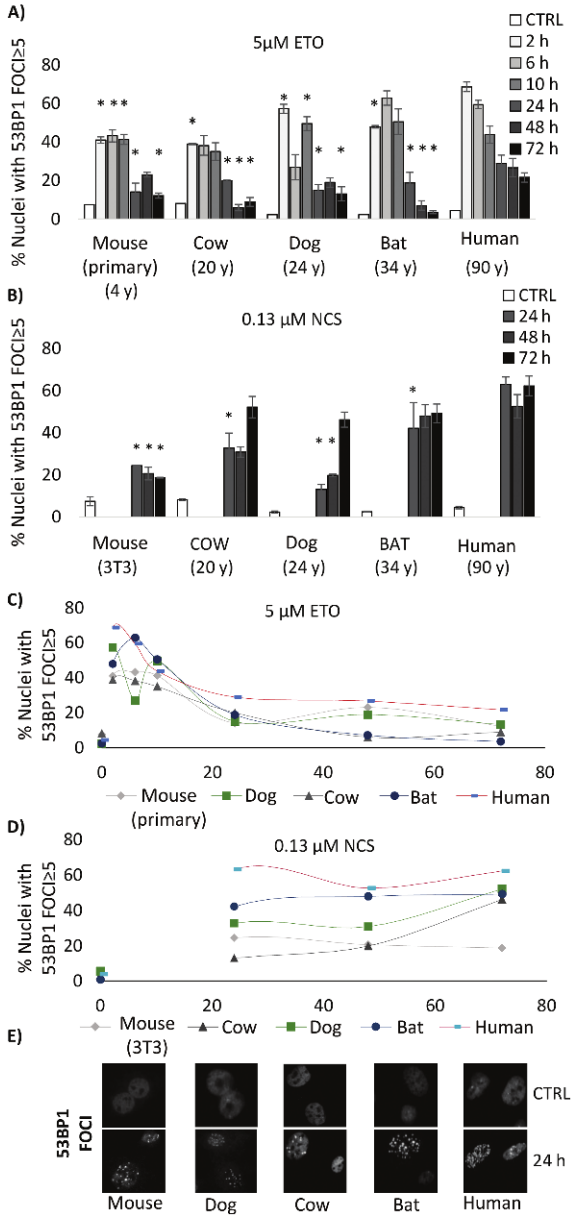

Figure 1. Long-lived species exhibit the highest percentage of p53 binding protein 1 (53BP1) foci. During S phase, cells were exposed to either 5 μM etoposide (ETO) or 0.13 μM neocarzinostatin (NCS) in serum-free medium. After treatment, cells were washed and fed with regular growth medium (10% fetal bovine serum). The respective maximum life span of each species is reported in parenthesis in years. (**A**) 5 μM ETO– treated cells were fixed either during and right after treatment at the following time points: 2, 6, 10, 24, 48, or 72 hours following the beginning of damage and stained for 53BP1 antibody. (**B**) 0.13 μM NCS treated cells were fixed at 24, 48, and 72 hours after the beginning of damage. Untreated fibroblasts were included as controls. From 200 to 400 cells per time point were counted and means ± *SEM* were calculated from two to six experiments. Cells scored for 53BP1 foci (*F*) were grouped into: $F < 5$, $5 \le F < 20$, and $F \ge 20$ foci per nucleus. The histogram bars show the percent of nuclei with 53BP1 foci ≥ 5 (obtained summing $5 \le F < 20$ and $F \ge 20$). Statistical significance (*$p < .05$) is referred to the comparison of all the species to the equivalent time point in human. Statistical analysis: analysis of variance followed by Tukey's multiple comparison test. Time course curves show the trend of foci formation after 5 μM ETO (**C**) and 0.13 μM NCS (**D**) treatment, in all species, from 0 to 72 hours. (**E**) Representative immunofluorescence image of 53BP1 foci formation in CTRL and 5 μM ETO–treated human cells, observed 24 hours after the beginning of damage.

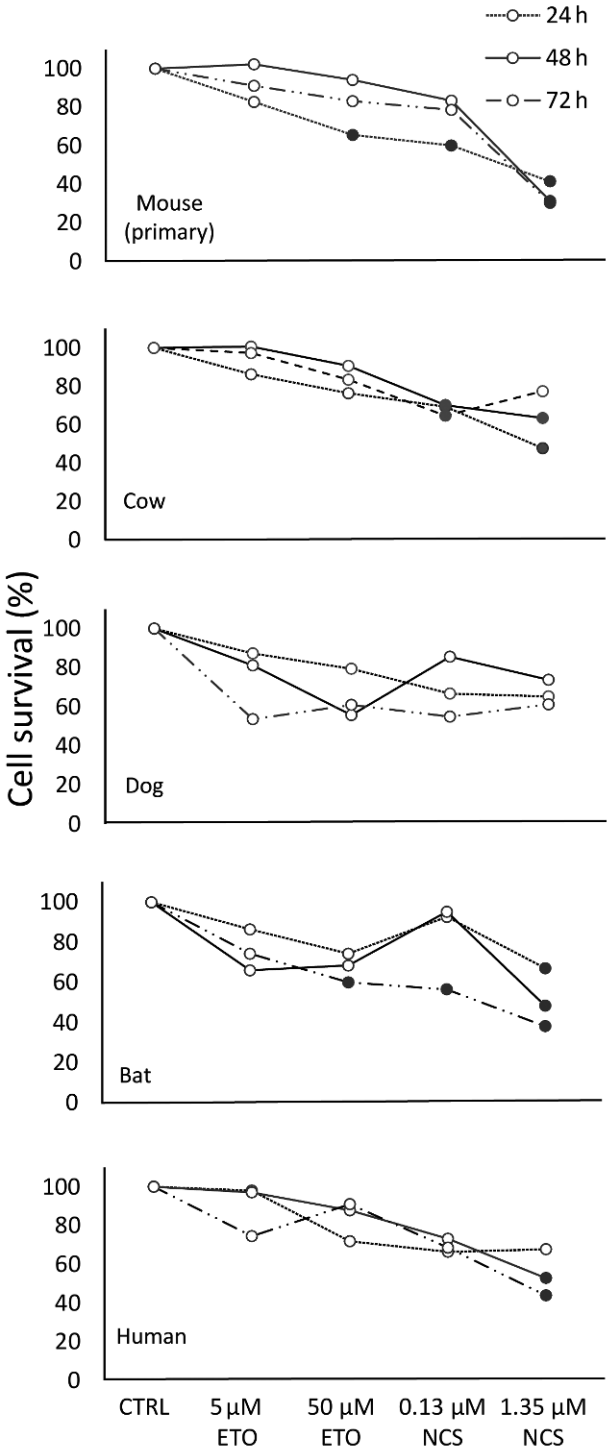

Figure 2. Low-dose treatments induce a low cytotoxic effect in all species. Fibroblast viability was evaluated with the colorimetric MTT assay in untreated (CTRL) and treated cells (5 and 50 μM etoposide [ETO]; 0.13 and 1.35 μM neocarzinostatin [NCS]) at 24, 48, and 72 hours after the beginning of treatment. Statistical analysis: analysis of variance (ANOVA) followed by Tukey's multiple comparison test ($p < .05$). ANOVA has been performed comparing treated sample to control cells at the relative time point. ● = $p < .05$; ○ = $p > .05$.

hundred 53BP1 foci, more than 80 colocalized with γ-H2AX in both species (Supplementary Figure 3B). Similar and higher levels of colocalization were also observed in experiments where unsynchronized

human and 3T3 mouse cells were treated with NCS (for human cells, see Supplementary Figure 1E, data not shown for mouse 3T3 cells).

DNA Damage Induces Cell Cycle Arrest

Progression through the cell cycle was monitored by cytofluorimetric measurement of DNA content in mouse, dog, cow, and human cells (Supplementary Figure 4). Cyclin A and Nek 4 expression was examined in species for which antibodies with conserved epitopes were available. These species included mouse, cow, little brown bat, and human (Supplementary Figure 5). Cytofluorimetric analysis revealed a significant shift in the cell cycle profile in all four species tested. In treated cells, there was an increased percentage of cells in the S and G_2 phases of the cell cycle, especially G_2 in mouse and S in dog, cow, and human. Increased expression in cyclin A in all treated cells confirmed a larger proportion of cells in G_2 arrest. This was evident in all species, but especially pronounced in human and cow. In addition, the expression of Nek 4, a recently described regulator of both DNA-PK association with DNA damage and entry into senescence (22), also increased following damage.

To better observe differences in the efficiency of cell cycle arrest following damage, we exposed mouse and human cells to 5 μM ETO and pulsed them with BrdU. Cells were analyzed for the percentage of cells synthesizing DNA (BrdU-positive nuclei) and the percentage that harbor BrdU-positive 53BP1 foci (BrdU staining only in damage foci) at time points from 14 to 72 hours after the beginning of damage. At 14 hours, human cell populations contained a lower percentage of cells synthesizing DNA compared with mouse cells, but a similar percentage of cells with BrdU foci. At 24 hours, the percentage of cells incorporating BrdU increased for both species, indicating progression through the cell cycle. Again, the human population had a lower percentage of cells incorporating BrdU, but a higher percentage of BrdU in foci, suggesting a more active repair (Supplementary Figure 6).

DNA Fragility Across Species

We next evaluated DNA fragility after genotoxic stress. We performed comet assays under neutral conditions for the detection of DNA damage at the level of the individual cell. Comet tails obtained with 5 μM ETO and 0.13 μM NCS, the concentrations used in long-term experiments, were too short to measure significant differences (data not reported). For this reason, higher doses of ETO and NCS were used for comet assays. Figure 3 contains data from cells treated with 50 μM ETO and 1.35 μM NCS for 60 and 30 minutes, respectively. Genotoxic treatments resulted in DNA fragmentation and the appearance of comet tails. We calculated fold increase in the percentage of DNA in comet tails and in tail moments (measures obtained by multiplying tail length by percentage DNA in tail). After both treatments, we observed a significant increase in the percentage of tail DNA in all species. Although the results of the two measure of DNA damage (percent tail DNA and tail moment) did not overlap, cells from the mouse, the shortest-lived species in the panel, had significantly greater DNA fragmentation in all instances. The longest-lived species (human) and the largest species (cow) exhibited the least amount of damage in the comet assay. Because DNA damage repair is activated within minutes of damage (23), we expect that fast repair mechanisms rather than chromatin structural strength are responsible for the observed differences among species.

Measuring Unresolved Damage

To assess the amount of unresolved damage in each species after genotoxic stress, we scored micronuclei formation 0, 24, 48, and

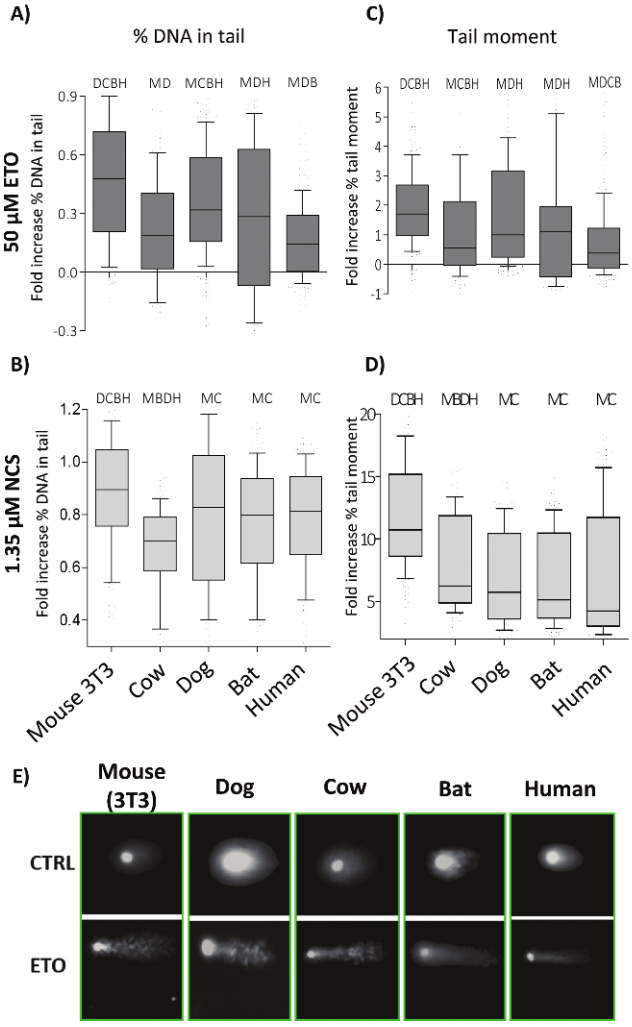

Figure 3. Human DNA generally appears more or equally resistant to fragmentation when compared to other species. Quantification of percent DNA in comets tails (**A** and **B**) and quantification ofTail moment (**C** and **D**) after 50 μM etoposide (ETO) and 1.35 μM neocarzinostatin (NCS) are presented in a box plot showing means ± *SEM* and whiskers representing 10–90 percentile. For both treatments, data were obtained from two independent experiments. Statistical analysis: Kruskal–Wallis analysis. These data from a single species were compared to each individual species. Significant difference ($p < .0001$) between pairs of species is indicated by the presence of the initials above the box plot for each species (M = mouse; D = dog; C = cow; B = bat; H = human). (**E**) Representative comets of untreated (CTRL) and 50 μM ETO–treated fibroblasts.

72 hours after the beginning of damage. Micronuclei originate from chromosome fragments or whole chromosomes that lag behind at anaphase (17). We observed that shorter-lived species have a higher percentage of nuclei with ≥1 micronucleus. In particular, mouse, the shortest-lived species, showed the highest percentage of micronuclei at all time points both after 5 μM ETO and 0.13 μM NCS treatments (Figure 4A and B, respectively). As a demonstration that micronuclei arise only in cycling cells, we also scored them in BrdU-positive cells (Figure 4C). The steady state level of the 53BP1 protein was also assessed following genotoxic stress. Independently from treatment time, whole lysates show a multiband pattern of 53BP1, suggesting the existence of different modifications of the protein (Supplementary Figure 7A). Densitometric analysis of multiple experiments including all four visible bands is shown in Supplementary Figure 7B.

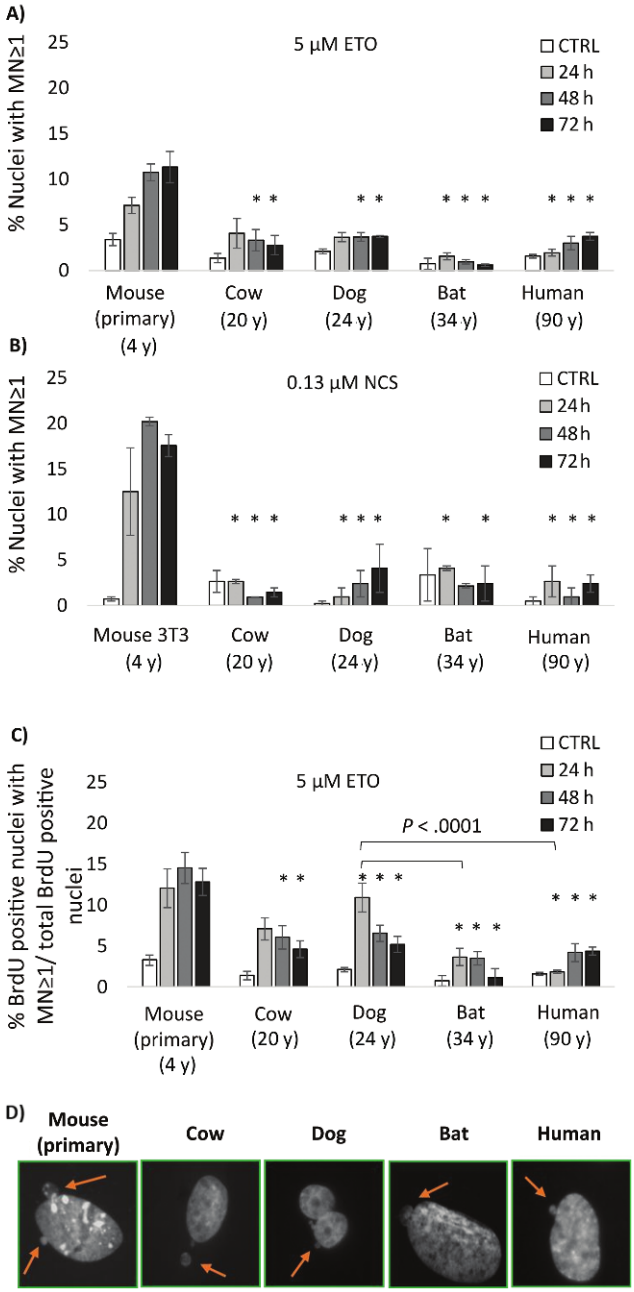

Figure 4. Short-lived species have higher percentage of micronuclei (MN). All cells were synchronized in G_0 phase by 48-hour incubation in serum-free medium. Cells were then stimulated to enter into the S phase by adding complete growth medium (10% fetal bovine serum) as described in Material and Methods section. Cells in S phase were treated in serum-free medium with 5 µM etoposide (ETO; **A**), 0.13 µM neocarzinostatin (NCS; **B**), or 5 µM ETO with a BrdU pulse (**C**; cells were pulsed with BrdU for all the length of the treatment); cells were washed and fed with growth medium and allowed to recover from damage. Micronuclei were scored at 24, 48, and 72 hours after the beginning of the treatment. Means ± *SEM* of the percentage of nuclei with MN > 1, scored on a minimum of 400 cells, are presented. Means were calculated from two to six experiments. In all instances, control cells (CTRL) are cells at 24-hour past complete growth medium addition. The respective maximum life span of each species is reported in parenthesis in years. Statistical significance ($p < .05$) is reported by an asterisk (*) for comparisons of each species to the equivalent time point in mouse or ($p < .0001$) with square brackets between other species. Statistical analysis: analysis of variance followed by Tukey's multiple comparison test.

It appears that protein levels do not change substantially during the 24 hours following the beginning of 5 µM ETO treatment (except for the 24-hour time point in dog cells). This suggests that 53BP1 is a constitutive protein. Mouse and dog cells have significantly lower level compared with human cells. More generally, the larger and/or longer-lived species (cow, bat, and human) appear to possess higher 53BP1 protein amounts although these differences are always below onefold.

53BP1 Foci Are Inversely Correlated With Micronuclei Abundance

Long-lasting foci are interpretable as DNA Segments of Chromatin Reinforcing Senescence (abbreviated in SCARS) as suggested by Rodier and colleagues (24). In support of this interpretation, we have performed on human cells immunofluorescence experiments costaining for PML and for 53BP1. Supplementary Figure 8 shows that, even with the lowest concentration used, a significant increase in the percentage of PML nuclear body contiguous to 53BP1 foci is observable at 72 hours after the beginning of treatment.

To interpret the relationship between 53BP1 foci, micronuclei, and life span, we plotted the data for 53BP1 foci formation and micronuclei, with species longevity. We used data from the 72-hour time point following the beginning of NCS exposure because this treatment produces the highest number of long-lasting foci interpretable as SCARS. Micronuclei were inversely related to long-lasting foci (R^2 = .87; p = .021; Supplementary Figure 9A). In addition, long-lasting foci were strongly and positively related with longevity (R^2 = .87; p = .020; Supplementary Figure 9B), whereas micronuclei were negatively related (R^2 = .59), although this relationship did not reach significance in this data set (Supplementary Figure 9D). Like maximum life span, body mass was also positively related with long-lasting foci (R^2 = .36; Supplementary Figure 9C) and negatively related with micronuclei (R^2 = .35; Supplementary Figure 9E), although neither association reached significance in this data set. These data suggest that both longevity and body mass are related to genome surveillance and stability but that longevity is more strongly related than body mass.

Discussion

The aim of the present study is to understand the biological significance of the appearance of a higher number of DNA damage–induced 53BP1 foci in human cells compared to mouse cells (9). This initial finding was counterintuitive because a higher number of foci are generally interpreted as evidence of a greater amount of damage. However, using direct measurements of DNA damage such as the comet assay (Figure 3) and micronuclei counts (Figure 4), we report here that longevity and, to a lesser extent, adult body size are indeed associated with higher genomic stability. To explain this apparent contradiction between the direct measurement of DNA damage and 53BP1 foci count, we propose the following model graphically described in Figure 5:

> In mammals, DNA and associated proteins (histones) are chemically equivalent and similarly fragile when exposed to the same genotoxic damage. In a single species, 53BP1 foci abundance is proportional to the amount of damage. However, the difference observed in foci abundance between species is not due to different levels of damage but to different

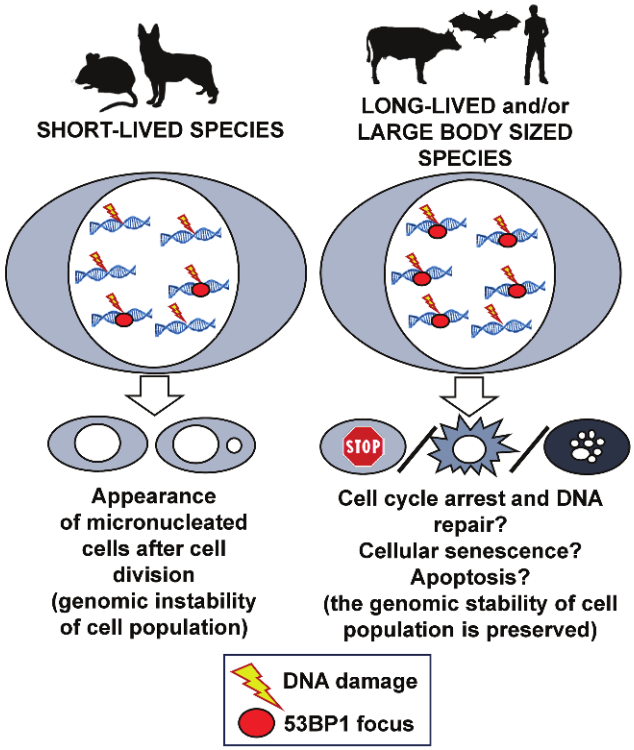

Figure 5. Proposed model. Solid dots represent p53 binding protein 1 (53BP1) foci, whereas lightning images represent DNA damage. See Discussion section for model explanation.

capacities to detect this damage. We suggest the possibility that foci represent a primary DNA damage response. Thus, within each species, a larger amount of damage correlates with an increase in the number of foci. However, when between-species comparisons are made, longer-lived or larger species produce more foci for a similar amount of DNA damage because they are more efficient in this primary DNA damage response. A potential downstream consequence of this difference is that long-lived or larger species may be more prone to activate cell cycle arrest and DNA repair, apoptosis, or senescence. The choice between these options will likely depend on the interactions between the level of damage and other cellular and extracellular conditions.

The presence of 53BP1 foci was studied in a large investigation of skin-derived fibroblasts from 100 human donors aged 20–90 years. It was observed a positive correlation between donor age and 53BP1 foci and also a positive correlation between 53BP1 foci and micronuclei in support of the concept that, inside a single species, 53BP1 represents a marker of the endured DNA damage (25). An additional hypothesis that can be proposed following the reasoning of our model is that inside a cell population challenged with a genotoxic stress, cells with the least 53BP1 foci response will be the one more prone to genotoxic damage. Our data on foci abundance in micronucleated cells and in cells showing irregular nuclear architectures do not support this second hypothesis suggesting that the failed cellular mechanism responsible for micronuclei production and for nuclear abnormalities is downstream from 53BP1 foci formation (Supplementary Figures 1 and 2).

In support of our general model, we find that species with significant longevity (human and little brown bat) and species with a combination of moderate longevity and large adult body size (cow) demonstrate a higher level of early repair as measured by the comet assay. In addition, mouse, the species in our study in which short life span associates with small body mass, shows a significantly higher level of micronuclei compared with all other longer-lived or larger species. Concerning 53BP1 foci abundance, mouse cells and to a lesser extent cow cells produce fewer foci after damage compared with the other species. Little brown bat and human, the two species with the longest life span, show the highest level of foci both at shorter time points (see 5 μM ETO treatment) and at longer time points (see 0.13 μM NCS treatment).

Rodier and colleagues have suggested to consider persistent foci (ie, foci that have not resolved in 24 hours) as DNA SCARS (24). Our data on PML contiguity with 53BP1 in human cells supports this proposal. DNA damage–induced cellular senescence and apoptosis, in association with more proficient cell cycle checkpoints, could be effective ways to guarantee tissue's genomic stability when multiple cellular divisions are required to provide sufficient tissue turnover during a long life span or attain a large body size (eg, see ref. (26)). More data are needed to investigate these not-mutually exclusive possibilities.

In this study, both primary and immortalized mouse cells have been used. Immortalization may have an impact on cell cycle time and checkpoint efficiency. The present work, however, in conjunction with our previous data where a comparison between primary mouse and human fibroblasts in their response to NCS was performed (9), shows that immortalization does not alter significantly the 53BP1 foci and micronuclei response to genotoxic damage, at least in mouse. Similarly, not relevant differences were observed comparing primary cells from adult or embryo origin (data were available only for human and mouse). These data are in line with our previous observations on DNA-end binding that show similar high levels of this activity for primary human fibroblasts (embryo or adult derived) and HeLa cells (10). The invariability of these cellular responses with the developmental stages of the tissue of origin and with immortalization suggests that they represent fundamental biological characteristic of a species.

Although our investigation includes a small number of species, we have chosen a set of species with a wide range in maximum life span and adult body mass in an attempt to dissociate the potential effects of these two parameters on genome stability. Species longevity and body mass are known to correlate with each other (27), and it is reasonable to expect that they both correlate positively with genome stability. The common mammalian ancestor was small sized and probably short lived (ref. (28) and references therein). It is reasonable to suggest that a variety of mechanisms have evolved to ensure the genomic stability required for larger body size and longer life span. Some of these mechanisms will be important especially for long-lived species, whereas others will be important especially for species with large bodies (eg, see ref. (29)); moreover, some will be common to several (or perhaps all) species, whereas others will be unique to particular orders, families, or species. We believe, interpreting the present study in the context of our previous observation on DNA-end binding (10), that improving DNA damage detection could be an evolutionarily recurrent mechanism to provide the increased genomic stability required in long-lived and large species to prevent, respectively, early-life tissue dysfunctions and tumor development. The relevance of this observation goes beyond the aging field because scientists studying DNA repair pathways commonly use cells lines derived from multiple

species. In addition, DNA damage foci are already studied at the clinical level as potential markers for radiosensitivity of tumors (30) and of patients' normal tissues (31). Clinicians, therefore, will have to interpret correctly the data obtained by researcher using different species to design the most adapted therapy for humans.

Supplementary Material

Supplementary data is available at *The Journals of Gerontology, Series A: Biomedical Sciences and Medical Sciences* online.

Funding

This work was supported by RFO 2014 of University of Bologna to A. Lorenzini, Fondazione del Monte di Bologna e Ravenna grant to C. Stefanelli, and National Institutes of Health/National Institute on Aging (grant AG39799) to C. Sell.

Acknowledgement

We thank Leslie Sell, PhD, for editorial assistance.

References

1. Kakarougkas A, Jeggo PA. DNA DSB repair pathway choice: an orchestrated handover mechanism. *Br J Radiol*. 2014;87:20130685. doi:10.1259/bjr.20130685
2. Mao Z, Bozzella M, Seluanov A, Gorbunova V. Comparison of nonhomologous end joining and homologous recombination in human cells. *DNA Repair (Amst)*. 2008;7:1765–1771. doi:10.1016/j.dnarep.2008.06.018
3. Rothkamm K, Krüger I, Thompson LH, Löbrich M. Pathways of DNA double-strand break repair during the mammalian cell cycle. *Mol Cell Biol*. 2003;23:5706–5715. doi:10.1128/MCB.23.16.5706-5715.2003
4. Rothkamm K, Barnard S, Moquet J, Ellender M, Rana Z, Burdak-Rothkamm S. DNA damage foci: meaning and significance. *Environ Mol Mutagen*. 2015;56:491–504. doi:10.1002/em.21944
5. Dimitrova N, Chen YC, Spector DL, de Lange T. 53BP1 promotes non-homologous end joining of telomeres by increasing chromatin mobility. *Nature*. 2008;456:524–528. doi:10.1038/nature07433
6. Wang B, Matsuoka S, Carpenter PB, Elledge SJ. 53BP1, a mediator of the DNA damage checkpoint. *Science*. 2002;298:1435–1438. doi:10.1126/science.1076182
7. Cescutti R, Negrini S, Kohzaki M, Halazonetis TD. TopBP1 functions with 53BP1 in the G1 DNA damage checkpoint. *EMBO J*. 2010;29:3723–3732. doi:10.1038/emboj.2010.238
8. Fernandez-Capetillo O, Chen H, Celeste A, et al. DNA damage-induced G 2—M checkpoint activation by histone H2AX and 53BP1. 2002;4:993–998. doi:10.108/ncb884
9. Fink LS, Roell M, Caiazza E, et al. 53BP1 contributes to a robust genomic stability in human fibroblasts. *Aging*. 2011;3:836–845. doi:10.18632/aging.100381
10. Lorenzini A, Johnson FB, Oliver A, et al. Significant correlation of species longevity with DNA double strand break recognition but not with telomere length. *Mech Ageing Dev*. 2009;130:784–792. doi:10.1016/j.mad.2009.10.004
11. Soubeyrand S, Pope L, Haché RJ. Topoisomerase IIalpha-dependent induction of a persistent DNA damage response in response to transient etoposide exposure. *Mol Oncol*. 2010;4:38–51. doi:10.1016/j.molonc.2009.09.003
12. Goldberg IH. Free radical mechanisms in neocarzinostatin-induced DNA damage. *Free Radic Biol Med*. 1987;3:41–54. doi:10.1016/0891-5849(87)90038-4
13. Dostál L, Kohler WM, Penner-Hahn JE, Miller RA, Fierke CA. Fibroblasts from long-lived rodent species exclude cadmium. *J Gerontol A: Biol Sci Med Sci*. 2015;70:10–19. doi:10.1093/gerona/glu001
14. Lorenzini A, Tresini M, Austad SN, Cristofalo VJ. Cellular replicative capacity correlates primarily with species body mass not longevity. *Mech Ageing Dev*. 2005;126:1130–1133. doi:10.1016/j.mad.2005.05.004
15. Gibson GE, Tofel-Grehl B, Scheffold K, Cristofalo VJ, Blass JP. A reproducible procedure for primary culture and subsequent maintenance of multiple lines of human skin fibroblasts. *Age (Omaha)*. 1998;21:7–14. doi:10.1007/s11357-998-0002-z
16. Gorczyca W, Gong J, Ardelt B, Traganos F, Darzynkiewicz Z. The cell cycle related differences in susceptibility of HL-60 cells to apoptosis induced by various antitumor agents. *Cancer Res*. 1993;53:3186–392.
17. Thomas P, Fenech M. Cytokinesis-block micronucleus cytome assay in lymphocytes. *Methods Mol Biol*. 2011;682:217–234. doi:10.1007/978-1-60327-409-8_16
18. Olive PL, Banáth JP. The comet assay: a method to measure DNA damage in individual cells. *Nat Protoc*. 2006;1:23–29. doi:10.1038/nprot.2006.5
19. Gyori BM, Venkatachalam G, Thiagarajan PS, Hsu D, Clement MV. OpenComet: an automated tool for comet assay image analysis. *Redox Biol*. 2014;2:457–465. doi:10.1016/j.redox.2013.12.020
20. Mosmann T. Rapid colorimetric assay for cellular growth and survival: application to proliferation and cytotoxicity assays. *J Immunol Methods*. 1983;65:55–63. doi:10.1016/0022-1759(83)90303-4
21. Nikolova T, Dvorak M, Jung F, et al. The γH2AX assay for genotoxic and nongenotoxic agents: comparison of H2AX phosphorylation with cell death response. *Toxicol Sci*. 2014;140:103–117. doi:10.1093/toxsci/kfu066
22. Nguyen CL, Possemato R, Bauerlein EL, Xie A, Scully R, Hahn WC. Nek4 regulates entry into replicative senescence and the response to DNA damage in human fibroblasts. *Mol Cell Biol*. 2012;32:3963–3977. doi:10.1128/MCB.00436-12
23. Mari PO, Florea BI, Persengiev SP, et al. Dynamic assembly of end-joining complexes requires interaction between Ku70/80 and XRCC4. *Proc Natl Acad Sci USA*. 2006;103:18597–18602. doi:10.1073/pnas.0609061103
24. Rodier F, Muñoz DP, Teachenor R, et al. DNA-SCARS: distinct nuclear structures that sustain damage-induced senescence growth arrest and inflammatory cytokine secretion. *J Cell Sci*. 2011;124(Pt 1):68–81. doi:10.1242/jcs.071340
25. Waaijer MEC, Croco E, Westendorp RGJ, et al. DNA damage markers in dermal fibroblasts in vitro reflect chronological donor age. *Aging*. 2016;8:147–157. doi:10.18632/aging.100890
26. Lorenzini A, Fink LS, Stamato T, Torres C, Sell C. Relationship of spindle assembly checkpoint fidelity to species body mass, lifespan, and developmental rate. *Aging*. 2011;3:1206–1212. doi:10.18632/aging.100416
27. Austad SN. Diverse aging rates in metazoans: targets for functional genomics. *Mech Ageing Dev*. 2005;126:43–49. doi:10.1016/j.mad.2004.09.022
28. O'Leary MA, Bloch JI, Flynn JJ, et al. The placental mammal ancestor and the post-K-Pg radiation of placentals. *Science*. 2013;339:662–667. doi:10.1126/science.1229237
29. Croco E, Marchionni S, Lorenzini A. Genetic instability and aging under the scrutiny of comparative biology: a meta-analysis of spontaneous micronuclei frequency. *Mech Ageing Dev*. 2016;156:34–41. doi:10.1016/j.mad.2016.04.004
30. Willers H, Gheorghiu L, Liu Q, et al. DNA damage response assessments in human tumor samples provide functional biomarkers of radiosensitivity. *Semin Radiat Oncol*. 2015;25:237–250. doi:10.1016/j.semradonc.2015.05.007
31. Bourgier C, Lacombe J, Solassol J, et al. Late side-effects after curative intent radiotherapy: identification of hypersensitive patients for personalized strategy. *Crit Rev Oncol Hematol*. 2015;93:312–319. doi:10.1016/j.critrevonc.2014.11.004